Korean J. Chem. Eng., 32(5), 808-815 (2015)
DOI: 10.1007/s11814-014-0279-9

pISSN: 0256-1115
eISSN: 1975-7220

Adsorption breakthrough dynamics of zeolites for ethylene recovery from fluid catalytic cracking fuel-gas

Dooyong Park*, Eun-Ji Woo*, Ji Won Choi*, Hyungwoong Ahn, and Chang-Ha Lee*,†**

*Department of Chemical and Biomolecular Engineering, Yonsei University, Seoul 120-749, Korea
**Scottish Carbon Capture and Storage Centre, Institute for Materials and Processes, The University of Edinburgh, UK
(*Received 12 May 2014 • accepted 21 September 2014*)

Abstract−The adsorption dynamics of zeolite 13X, 10X and 5A beds was investigated for recovering ethylene (C_2H_4) from fluidized catalytic cracking fuel-gas. As a feed gas, a ternary mixture ($CH_4 : C_2H_4 : C_2H_6$) and a model FCC fuel-gas ($CH_4 : C_2H_4 : C_2H_6 : C_3H_6 : N_2 : H_2$) were used for breakthrough experiments. In the ternary mixture, the concentration profiles showed similar patterns in all zeolite beds. C_2H_4 showed higher adsorption affinity than the others in all zeolites and zeolite 5A had the highest adsorption capacity of C_2H_4. In the six-component mixture, the breakthrough curves in the zeolite 5A bed showed similar patterns to the results of the ternary mixture. Although weak adsorbates could be removed during the adsorption step, CH_4 and N_2 imparted a steric hindrance to the initial stage of C_2H_4 adsorption in the zeolite 5A bed. Since vacuum desorption contributed to producing a high purity of C_2H_4, a pressure vacuum swing adsorption process was recommended to recover C_2H_4.

Keywords: Zeolite, Adsorption, FCC Fuel-gas, Ethylene, C_2H_4, PVSA

INTRODUCTION

Olefin and paraffin are widely used as a feedstock, but they are mainly produced as a mixture of paraffin/olefin. Therefore, it is important to have a process to separate olefin from paraffin. A low-temperature distillation (cryogenic) process has been used for many years. However, since this conventional process requires high investment cost, operating cost and energy cost, it is not always possible to justify this process of producing olefin from an economic standpoint.

C_2H_4 and C_3H_6 are the two most important bulk products of petrochemical industries. Fluid catalytic cracking (FCC) fuel-gas contains significant amounts of light olefin, on the order of 13-20 mol% C_2H_4. This fuel-gas also contains 30-35 mol% simple gases, such as H_2 and N_2, and typically more than 30 mol% CH_4. The C_2H_4 recovery from the fuel-gas has been also performed conventionally by low temperature and/or high pressure distillation. Therefore, it is essential to develop a novel process for this separation to conserve energy. For this reason, adsorption technologies have received considerable attention as a strong candidate technology to recover C_2H_4 from FCC fuel-gas [1-3].

Adsorptive separation processes are particularly viable alternatives because the process allows one to increase the separation factor between olefin and paraffin, resulting in a cost reduction of the separation process. Commercially available adsorbents such as silica gel, alumina, activated carbon and zeolite have been evaluated in the adsorption processes. Zeolite, in particular, has been a major contender as the primary adsorbent for light hydrocarbon separation due to its high selectivity in the low pressure range. In addition, the divalent cations in zeolites function as strong adsorptive centers and they can interact with a strong quadrupole moment of C_2H_4, which enhances the recovery of C_2H_4 from light hydrocarbon mixtures [4-6]. For C4 separation, a metal complex or metal ion impregnated adsorbents using π-complexation capabilities have also been developed to improve olefin/paraffin selectivity [7-9].

Pressure swing adsorption (PSA) processes have been widely applied for separation and purification of gas mixtures in petroleum refining and the petrochemical industry due to its low energy consumption and high efficiency. The PSA process has demonstrated great capability to produce H_2 from various mixtures [10, 11]. Furthermore, the possibility of propylene recovery using PSA has also been reported [12]. However, to recover propylene in the adsorbed phase as a product, or to improve the efficiency, a vacuum is applied to the process, referred to as vacuum swing adsorption (VSA), even though the addition of a vacuum increases the energy requirements [13]. It was reported that a VSA process using silver nitrate impregnated clay adsorbent could adequately separate C_2H_4 from an C_2H_4/C_2H_6 mixture [2]. If fuel-gas can be supplied to the adsorption process, the pressure vacuum swing adsorption (PVSA) process can improve the separation efficiency without any additional compression energy [13,14]. Moreover, when the adsorbed component is strongly adsorbed, hot inert gas is often supplied to the adsorptive process (temperature swing adsorption; TSA) even though this increases the consumption of thermal energy [15].

For a well-designed PSA process, it is necessary to establish the characteristics of adsorption and desorption dynamics. Breakthrough experiments can provide basic information regarding adsorption and desorption dynamics [10,11]. Adsorbent characteristics and

†To whom correspondence should be addressed.
E-mail: leech@yonsei.ac.kr
‡This article is dedicated to Prof. Hwayong Kim on the occasion of his retirement from Seoul National Univerisity.

separation performance of the adsorption bed can also be observed from breakthrough experiments.

We investigated the adsorption dynamics of C_2H_4 mixtures in the bed packed with zeolite through breakthrough experiments. Considering the pore size and cation of zeolite, three pelletized zeolites (zeolite 5A, 10X and 13X), which are commercially available, were selected. Their breakthrough characteristics were studied with a ternary ($CH_4 : C_2H_4 : C_2H_6$; 52.5 : 24.6 : 22.9 mol%) and a six-component mixture ($CH_4 : C_2H_4 : C_2H_6 : C_3H_6 : N_2 : H_2$; 32.0 : 15.0 : 14.0 : 2.0 : 12.0 : 25 mol%). The three-component mixture was studied to understand the dynamic behaviors of the C1-C2 mixture on the zeolite bed before using the six-component mixture, which had a composition that reflects that of FCC fuel-gas common in the petrochemical industry. The temperature profiles in zeolite beds were monitored to understand the dynamic characteristics of each component during adsorption, desorption by blowdown and/or vacuum, and re-adsorption using the six-component mixture. The results of the adsorption and desorption dynamics may contribute to the design of cyclic adsorption processes such as PSA, TSA and PVSA.

EXPERIMENT

Two different C_2H_4 gas mixtures were used as feeds. The ternary mixture ($CH_4 : C_2H_4 : C_2H_6$=52.5 : 24.6 : 22.9 mol%) consisted of major C1-C2 components contained in FCC fuel-gas so that it could contribute to understanding the adsorption characteristics of major carbon components. A six-component mixture ($CH_4 : C_2H_4 : C_2H_6 : C_3H_6 : N_2 : H_2$=32.0 : 15.0 : 14.0 : 2.0 : 12.0 : 25.0 mol%), which reflects the composition of actual FCC fuel-gas, was used. Zeolite 5A, 10X, and 13X were chosen as adsorbents and their characteristics are listed in Table 1.

A schematic diagram of the breakthrough experimental apparatus is shown in Fig. 1. The column was fabricated from a stainless steel pipe of 3.5 cm ID, 100 cm length, and 0.5 cm wall thickness. The amounts of adsorbent packed in the column were 722, 725.4 and 729.2±2 g for zeolite 5A, 10X and 13X respectively. Prior to the experiments, each adsorbent was activated at 350 °C for 12 hours. After the adsorbent was packed into the column, it was purged by H_2. Then, the adsorption bed was initially saturated with H_2 (99.9999+%) at 2 atm to protect adsorbents from outside contaminants [7]. Therefore, in the study, breakthrough experiments were in a clean bed condition.

Thermocouples were installed at several locations along the column to measure temperature variation during adsorption and desorption steps. A mass flow controller, calibrated by a wet gas meter was used to accurately control the feed flow rate. The adsorption pressure was fixed by a back pressure regulator that was installed

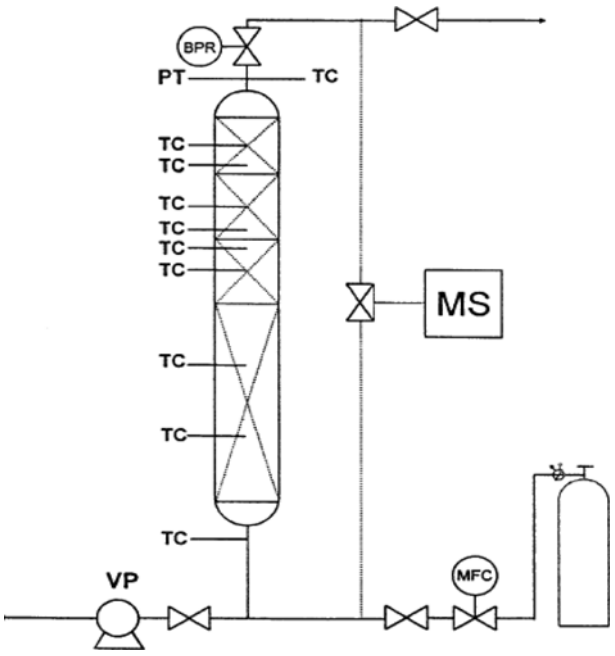

Fig. 1. Experimental apparatus for breakthrough experiment.
MS. Mass spectrometer MFC. Mass flow controller
TC. Thermocouple PT. Pressure transmitter
BPR. Back pressure regulator VP. Vacuum pump

at the top of the column. Feed and effluent concentrations were measured by a mass spectrometer (Balzers Quadstar™ 421) within ±0.1 mol% accuracy. To compare performance among the adsorbents, the feed rate and adsorption pressure were fixed at 4 LSTP/min and 4 atm, respectively.

After completion of the adsorption breakthrough experiment, the bed was used in the desorption study. First, desorption dynamics were studied by a blowdown step from 4 atm to 1 atm (that is, depressurization). Then, the best adsorbent with respect to adsorption capacity in the breakthrough experiments was tested with an additional desorption step under vacuum conditions because vacuum desorption led to the recovery of C_2H_4 of high-quality. Since the bed pressure was changed during the blowdown and vacuum desorption steps, the gas velocity in the bed slowed over time. As a result, the gas velocity could not be specified in these steps even though it was controlled by a valve, similar to the blowdown and vacuum steps in the PSA process.

RESULTS and DISCUSSION

1. Adsorption and Desorption Dynamics of a Ternary Mixture

The experimental breakthrough curves on a zeolite 13X bed using

Table 1. Characteristics of the adsorbents

	Type	Pellet size (cm)	Pellet density (g/cm^3)	Bed density (g/cm^3)	External void fraction	Heat capacity (cal/gca)
Zeolite5A	Granular	0.157	1.16	0.80	0.32	0.32
Zeolite10X	Pellet	0.115	1.10	0.82	0.31	0.42
Zeolite13X	Granular	0.105	0.93	0.69	0.25	0.42

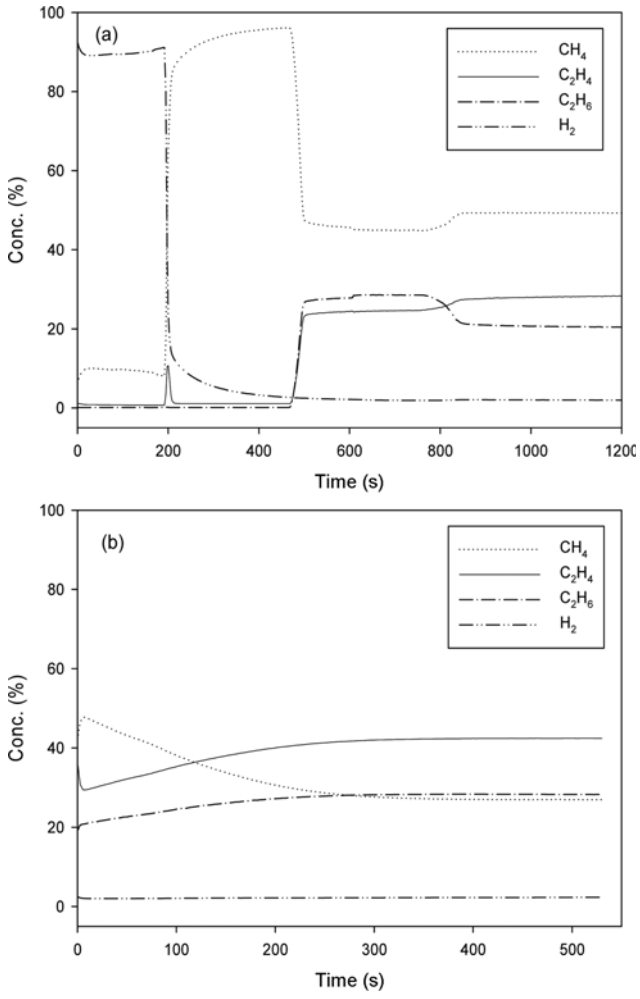

Fig. 2. Concentration profiles during (a) adsorption and (b) blowdown desorption in zeolite 13X bed with ternary mixture.

a ternary mixture ($CH_4 : C_2H_4 : C_2H_6$=52.5 : 24.6 : 22.9 mol%) are presented in Fig. 2. Since the bed was saturated by H_2 at 2 atm to protect adsorbents from outside contaminants, the bed was pressurized by the feed gas up to 4 atm before breakthrough experiments. Since H_2 is the weakest adsorbate in the feed used in the study, it is expected that H_2 molecules in pore and surface on zeolites can be replaced easily by the adsorption of other molecules [18]. In addition, even though CH_4 is a stronger adsorbate than H_2, it will also work as a weak adsorbate compared with other components (C_2H_4, C_2H_6, C_3H_6) in the feeds. For the initial period, therefore, levels of H_2 and CH_4 were observed because those components, which are weak adsorbates, moved to the bed end during the pressurization step.

CH_4 was the first breakthrough component, followed by C_2H_4 and C_2H_6 with about 300s intervals. The roll-up phenomenon of CH_4 and C_2H_6 results from the fact that weakly adsorbed components lose their adsorption sites due to the competitive adsorption of more strongly adsorbed components [12].

In the equilibrium-driven separation process, the effluent concentration of some components may exceed their steady inlet value in the breakthrough curve. This phenomenon is attributed to the displacement of the weakly adsorbed (or lighter) components by more strongly adsorbed (or heavier) components [11,14,15,20]. However, the difference in the sorption rate or the steric hindrance by pre-sorbed adsorbates in the pore mouth also contributes to the sorption dynamics and roll-up in the kinetic-driven separation process [21-24].

In the case of H_2, the breakthrough curve descended drastically with the steep breakthrough of CH_4 and then decreased slowly until the breakthrough of C_2H_4 occurred. The plateau of the CH_4 concentration profile showed a slightly increasing slope with a smooth decrease of H_2 concentration. This result implied that the adsorption of CH_4 was hindered by the strong adsorbates at the initial stage. In addition, a small peak of C_2H_4 was observed as the concentration of CH_4 increased. The micropore size of zeolite depends on the type of zeolite because zeolites are well-defined structural porous materials. However, since the zeolite pellet is made of zeolite crystals and binder, it showed two additional pores of 3.8 nm (pore size distribution: 3.1-4.4 nm) and 34.7 nm (pore size distribution: 18.7-61.4 nm) in average pore size. And the pore volumes were $1.8*10^{-2}$ cm^3/g and $1.0*10^{-1}$ cm^3/g, respectively.

Since the adsorption affinity of C_2H_4 is stronger than that of CH_4, this peak does not stem from the competitive adsorption between C_2H_4 and CH_4. In the study, molecules can be occupied in the mesopore and macropore of the zeolite pellet without any significant competitive adsorption among molecules because the mesopore and macropore space among zeolite crystals is made at pelletization. Therefore, it was presumed that a small amount of C_2H_4 also came out from mesopore and macropores of the zeolite pellet with CH_4 when the adsorbed CH_4 was desorbed by C_2H_4 and C_2H_6.

The concentration of C_2H_4 was slightly higher than that of C_2H_6 before the simultaneous breakthroughs of both components. However, the roll-up of C_2H_6 had occurred by C_2H_4. Therefore, the results implied that the adsorption affinity of C_2H_4 with the double bond is stronger than that of C_2H_6 in terms of equilibrium-driven separation, but its adsorption rate on zeolite 13X is slightly slower than C_2H_6 from the viewpoint of kinetic-driven separation. And the adsorption breakthrough curves were mainly affected by the equilibrium difference, but kinetic effects also contributed a little to the adsorption dynamics. This could be confirmed by blowdown desorption.

After the adsorption experiment, a desorption phenomenon was observed by applying the blowdown step to the adsorption bed saturated by the feed gas. The concentration of CH_4 was detected at about 50 mol% in the early stage and decreased gradually to about half of the feed composition because CH_4, a relatively weak adsorbate, came out from the bed void and adsorbents. The C_2H_4 desorption concentration increased gradually to more than 40 mol% due to its high adsorption selectivity, but the C_2H_6 desorption concentration was slightly higher than its feed concentration in Fig. 2(b). The result confirmed that a greater amount of C_2H_4 than C_2H_6 can be adsorbed and a certain amount of C_2H_6 is displaced by C_2H_4 adsorption due to higher adsorption affinity of C_2H_4. Therefore, the roll-up of C_2H_6 was naturally observed from the adsorption breakthrough result in Fig. 2(a). The result also indicated that CH_4 could not be fully replaced by the strong adsorbates, C_2H_4 and C_2H_6, in zeolite 13X during the adsorption step due to the steric hindrance.

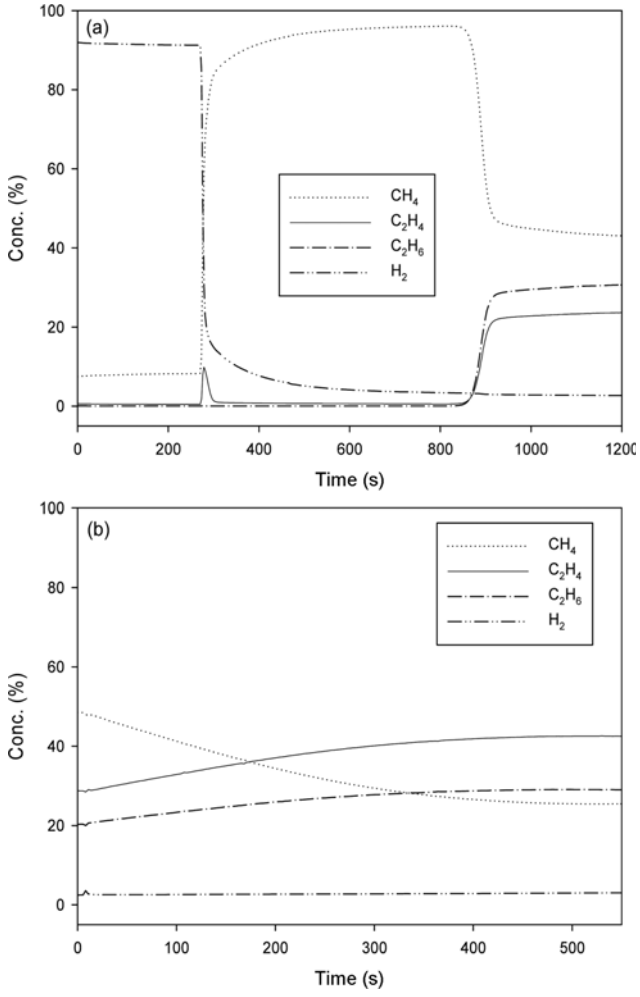

Fig. 3. Concentration profiles during (a) adsorption and (b) blowdown desorption in zeolite 10X bed with ternary mixture.

As a result, a certain level of CH_4 was occupied inside the adsorbents and CH_4 desorption took relatively a long time by simple depressurization.

The breakthrough curves in the zeolite 10X bed are shown in Fig. 3. The concentration profiles display trends similar to those of the zeolite 13X bed shown in Fig. 2, but the breakthrough time of each component was elongated. The breakthrough time of CH_4 was extended and the plateau of CH_4, which was more than 90 mol%, remained until 900 seconds, compared to the results of the zeolite 13X bed. Moreover, the breakthrough times of C_2H_4 and C_2H_6 were significantly longer and the roll-up of C_2H_6 was higher than those in the zeolite 13X bed. This behavior implied that the adsorption affinities and capacities of C_2H_4 and C_2H_6 in zeolite 10X were higher than those in zeolite 13X.

In Fig. 3(b), the desorption concentration profiles at the blowdown step show similar concentration profiles to those of the zeolite 13X bed. However, due to high adsorption capacity, the final concentration of C_2H_4 was higher than that in zeolite 13X during the blowdown desorption.

The breakthrough curves and blowdown desorption curves in the zeolite 5A bed are presented in Fig. 4(a) and (b). The breakthrough time of each component in the zeolite 5A bed was slightly higher than that in the zeolite 10X bed in Fig. 3(a) and (b). The difference in breakthrough time among adsorbents may have stemmed from the difference in both the adsorption equilibrium and the mass transfer resistance [13]. The difference in adsorption affinity between C_2H_4 and C_2H_6 was slightly higher in the zeolite 5A bed than in zeolite 10X bed.

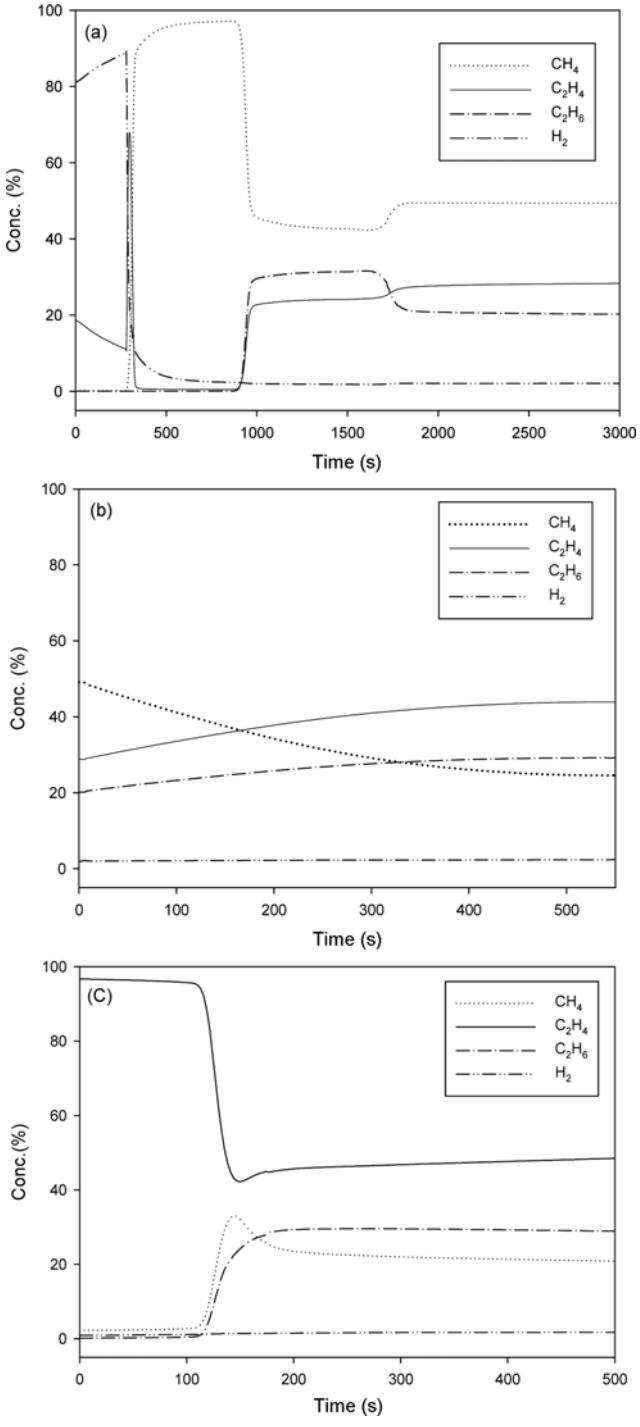

Fig. 4. Concentration profiles during (a) adsorption (b) blowdown and (c) vacuum desorption after the blowdown step in zeolite 5A bed with ternary mixture.

The main difference between zeolite 5A and the other beds was observed at the initial stage of the breakthrough curve. Compared to zeolite 10X and 13X beds, the C_2H_4 concentration was much higher than the CH_4 concentration at the initial stage, and the peak concentration of C_2H_4 at the CH_4 breakthrough point was much higher. The result implies that the π-bonded C_2H_4 does not easily pass through the pores of zeolite 5A, which has the smallest micropores in the study, during the pressurization step. The C_2H_4 in macropores, which occupied pore space and was not adsorbed in the micropore, flowed out through the bed with the quickly desorbed CH_4 from micropores and, thus, the peak concentration of C_2H_4 was observed at the initial stage. As a result, regardless of adsorption affinity, the adsorption rate of C_2H_4 in the micropores seemed to be slower on zeolite 5A than the other bed materials.

The breakthrough results showed that the adsorption of C_2H_4 was significantly stronger than C_2H_6 and C_2H_4 in the zeolite pores. It is reported that this effect must be due to the specific interactions between the C_2H_4 π-bonds and the cationic sites in the zeolite micropores [6]. In addition, according to the overall experimental results, it can be concluded that zeolite 5A is the most appropriate adsorbent for C_2H_4 adsorption among the three tested zeolites.

As shown in Fig. 4(b), the C_2H_4 concentration in the zeolite 5A bed during the blowdown desorption was slightly higher than the other zeolite beds. However, the blowdown step was not sufficient to recover the adsorbed C_2H_4, unlike the results in the other zeolites. Therefore, vacuum desorption was applied to the zeolite 5A bed after the blowdown desorption. And concentration profiles were presented in Fig. 4(c). However, the flow rate with time was significantly decreased during vacuum desorption. A trace amount of molecules was desorbed from about 100 seconds because the vacuum had already reached the desired pressure ($3.8*10^{-2}$ torr).

C_2H_4, with a concentration of up to 96 mol%, was produced during the initial stage of the vacuum step and its plateau continued for a certain period of time. When the desorption of C_2H_4 abruptly decreased, the concentrations of CH_4 and C_2H_6 increased; however, the concentration of C_2H_4 was still greater than the other components. After about 100 seconds, most adsorbed C_2H_4 had desorbed from the zeolite 5A bed on a molecular level. In summary, highly concentrated C_2H_4 could be recovered by vacuum swing adsorption. However, to improve the purity of recovered C_2H_4, the vacuum step time needed to be divided into two parts in the cyclic process design: production time and regeneration time.

2. Adsorption and Desorption Dynamics of the Six-component Mixture

The zeolite 5A bed showed the best performance among the tested zeolite beds to separate C_2H_4 from the ternary mixture. Therefore, the adsorption and desorption dynamics of the zeolite 5A bed was studied again by using a six-component mixture (CH_4 : C_2H_4 : C_2H_6 : C_3H_6 : N_2 : H_2; 32.0 : 15.0 : 14.0 : 2.0 : 12.0 : 25 mol%) which simulates the typical composition of FCC fuel-gas.

Fig. 5 shows the results of breakthrough and blowdown curves in the zeolite 5A bed. Since the mass spectrum of C_2H_4 and N_2 is identical in a mass spectrometer, the breakthrough curves of these gases were expressed in a combined curve.

In Fig. 5(a), the concentration profile of H_2 shows a similar roll-up phenomenon at the initial breakthrough period compared to the results of the ternary mixture in Fig. 4(a). However, the shapes of both roll-up profiles are a little different from each other, showing the H_2 roll-up before the breakthrough of C_2H_4+N_2 in FCC fuel-gas and before the breakthrough of C_2H_4 in ternary mixture. Note that the concentration profile of C_2H_4+N_2 in the six-component mixture shows a similar concentration profile of C_2H_4 in the ternary mixture at the early stage of adsorption, but the roll-up height and time of C_2H_4+N_2, as well as the inflection of the H_2 concentration profile are different from the result of the ternary mixture before the breakthrough of CH_4. These results imply that N_2 molecules, along with C_2H_4 molecules in the macropores, were transported out with CH_4 molecules at that time. The prominent roll-up of CH_4 was extended to the breakthrough time of C_2H_6 and the small roll-up of C_2H_4+N_2 profile was observed at the same time due to the breakthrough of C_2H_4. However, the breakthrough of C_3H_6 was not observed until 4,500 s. By using the adsorption process, H_2, N_2 and CH_4 can be removed from the FCC fuel-gas in the adsorption step. However, N_2 and CH_4 molecules may impart a steric hindrance effect on C_2H_4 adsorption at the initial stage of adsorption in the zeolite 5A bed. Moreover, since the adsorption

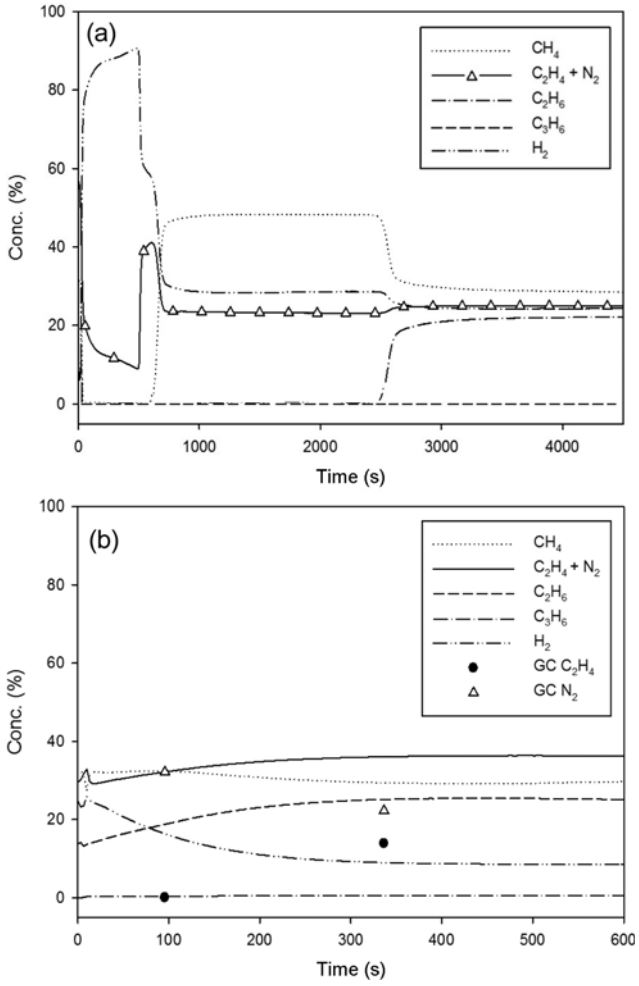

Fig. 5. Concentration profiles during (a) adsorption and (b) blowdown under 4 LSTP/min feed flow rate and 4 atm in the zeolite 5A bed with six-component gas mixture.

of C_3H_6 will occupy the adsorption sites strongly, this will lead to a decreased adsorption capacity of C_2H_4 and the difficulty of regenerating the zeolite 5A bed.

Fig. 5(b) shows concentration profiles during blowdown desorption. Gas chromatography (GC) was also used to analyze C_2H_4 and N_2, and each concentration of C_2H_4 and N_2 was described by symbols on the desorption curve. N_2 was mainly desorbed as shown in the desorption curve of C_2H_4+N_2 at the early stage followed by a gradual increase of the desorbed concentration of C_2H_4. Moreover, an increase of the C_3H_6 concentration was not observed. This result indicates that desorption of olefin (C_2H_4 and C_3H_6) is more difficult than other components simply through the depressurization of the zeolite 5A bed. Since C_2H_4 and C_3H_6 molecules were captured in the cages of zeolite 5A, vacuum desorption should be applied to the adsorption process as shown in the ternary mixture result in Fig. 4.

In the study, the six-component mixture contains a small amount of strong adsorbate (C_3H_6) as well as relatively weak adsorbates (N_2 and H_2) in the feed (CH_4 : C_2H_4 : C_2H_6 : C_3H_6 : N_2 : H_2=32.0 : 15.0 : 14.0 : 2.0 : 12.0 : 25.0 mol%). In addition, the mass-to-charge ratio of C_2H_4 and N_2 is identical and C1/C2 components are relatively dilute compared with the ternary mixture. As a result, it is difficult to determine the concentration profiles at the vacuum step and to evaluate the desorption characteristics. In the ternary mixture, the temperature excursion at the bed end agreed well with the breakthrough curves because the heats of adsorption reflect the adsorption amount and affinity [18]. Therefore, even though the propagation of temperature profiles is a little faster than that of MTZ, the dynamic behavior in the adsorption bed can be predicted indirectly by the temperature profiles [25,26]. We did not observe concentration profiles during vacuum desorption, but studied the temperature variation to elucidate the desorption indirectly.

Fig. 6 shows the temperature profiles during the breakthrough and blowdown steps in the zeolite 5A bed, which were located at 10, 50 and 80 cm from the feed end. One temperature excursion was observed at 10 cm because the mass transfer zone (MTZ) of each component was not separated at that position. However, through the propagation of MTZs, the temperature excursion was split into three parts, which might stem from the adsorption of N_2/CH_4, C_2H_6, and C_2H_4/C_3H_6, respectively. Then, the propagation length among the temperature peaks became more and more extended along the bed (80 cm) due to the difference of MTZ velocities. The temperature of each point decreased smoothly after an abrupt increase and the temperature profiles showed tailing due to the heat transfer effect.

As shown in Fig. 6(a), the maximum excursion reached 60 °C (40 °C increase), which implied the strong adsorption of C_2H_4 and C_3H_6 on zeolite 5A. On the other hand, the temperature variation at the blowdown desorption was relatively small, showing a 5 °C decrease along the bed. Moreover, no temperature excursion was observed. This highlighted the relatively weak adsorbates (N_2, CH_4, and C_2H_6), which were mainly desorbed by the blowdown step while C_2H_4 and C_3H_6 were still strongly adsorbed on zeolite 5A during depressurization. As a result, a vacuum step is required to produce the adsorbed olefins, but the purity of C_2H_4 will strongly depend on the concentration of C_3H_6.

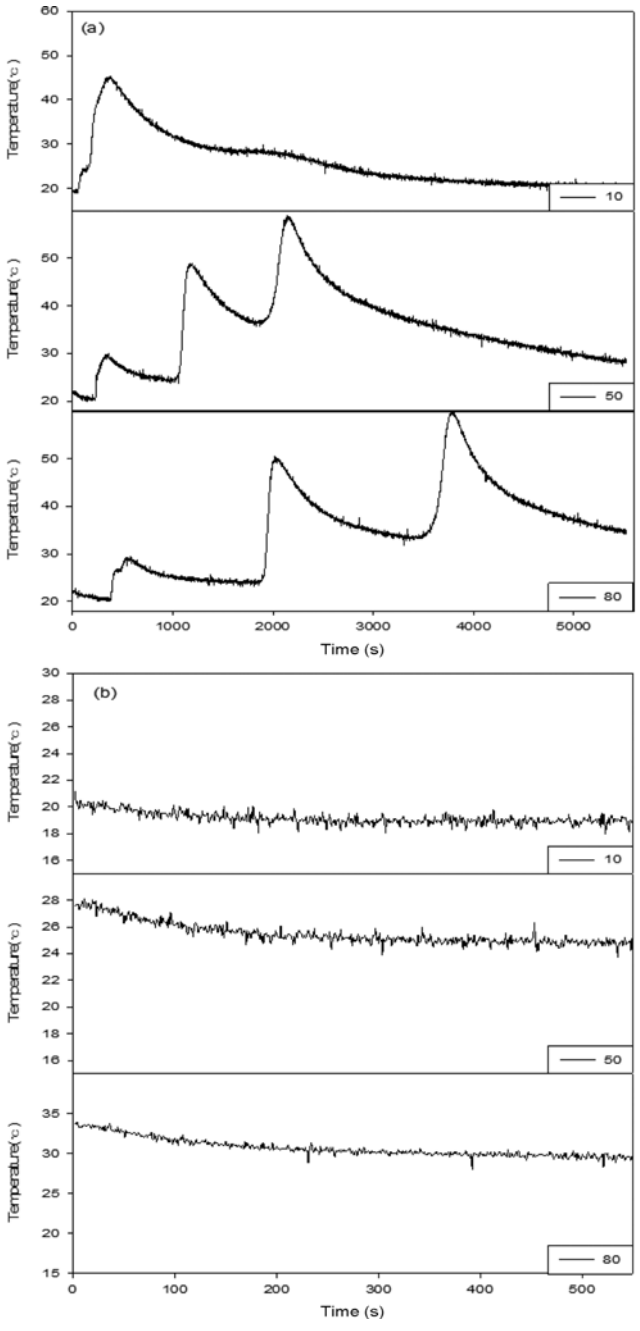

Fig. 6. Temperature profiles during (a) breakthrough adsorption and (b) blowdown desorption in zeolite 5A bed with six-component gas mixture.

Fig. 7 shows the temperature excursions of the re-adsorption breakthrough experiment after blowdown desorption in the zeolite 5A bed. The temperature increase was much smaller than that in Fig. 6(a). Moreover, a decrease in temperature profile was observed, showing two temperature peaks along the bed. Such temperature variations came from the replacement of weak adsorbates by the adsorption of strong adsorbates. Since the heats of adsorption and desorption occurred simultaneously, the temperature decrease indicated competitive adsorption/desorption among strong adsorbates, C_2H_4, C_2H_6 and C_3H_6. As a result, only a small amount

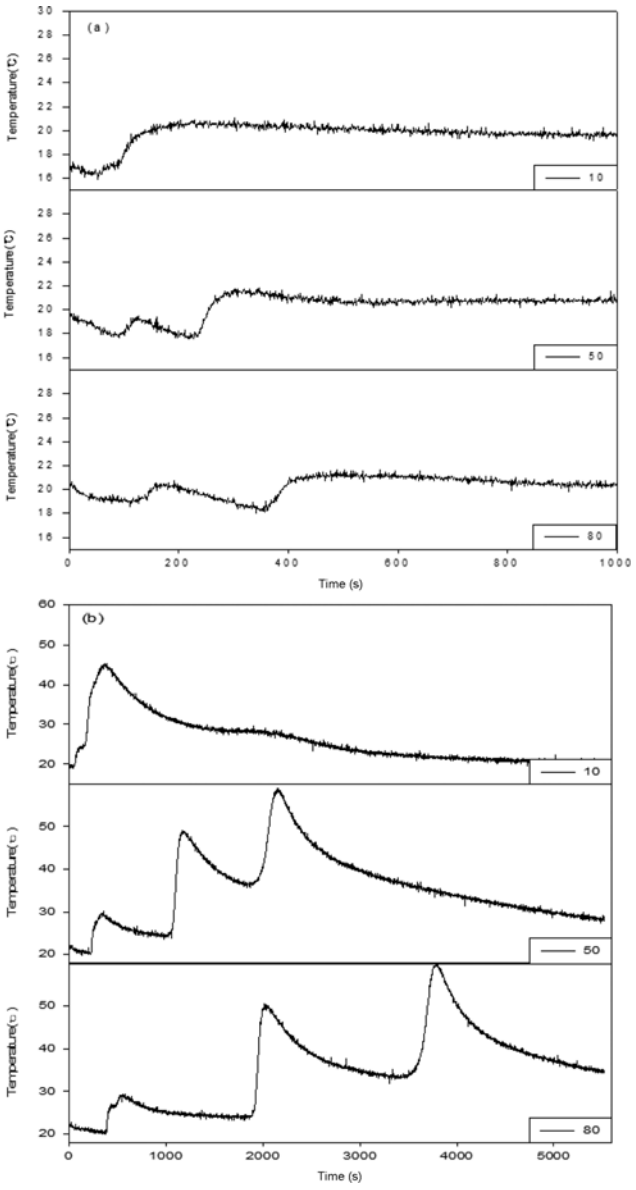

Fig. 7. Temperature profiles during re-adsorption after (a) blowdown desorption (b) blowdown and vacuum desorption in zeolite 5A bed with six-component gas mixture.

of the strong adsorbates could be replaced by the weak adsorbates because zeolite 5A was almost saturated by the strong adsorbates even after blowdown desorption. On the other hand, the temperature profiles of adsorption in the zeolite 5A bed regenerated by the blowdown and vacuum desorption were similar to Fig. 6(a), but the duration of the temperature excursion was shorter.

According to the results from the ternary and six-component mixtures, a rinse step by the product (C_2H_4) may be needed to improve product quality in a cyclic process. In addition, pressure vacuum swing adsorption (PVSA) using zeolite 5A is recommended to recover C_2H_4 from the FCC fuel-gas. Furthermore, even though the concentration of C_3H_6 in the feed is small, it can have a significant effect on the efficiency of the overall separation process using zeolite 5A.

CONCLUSION

The adsorption and desorption dynamics in zeolite 5A, 10X and 13X beds were studied to recover C_2H_4 from the FCC fuel-gas mixture by using a ternary mixture ($CH_4 : C_2H_4 : C_2H_6$; 52.5 : 24.6 : 22.9 mol%) and a six-component mixture ($CH_4 : C_2H_4 : C_2H_6 : C_3H_6 : N_2 : H_2$; 32.0 : 15.0 : 14.0 : 2.0 : 12.0 : 25 mol%).

The breakthrough curves in the ternary mixture showed similar patterns in all adsorbent beds. The breakthrough of CH_4 occurred first with a drastic decrease of H_2 concentration followed by those of C_2H_6 and C_2H_4. The breakthroughs of C_2H_4 and C_2H_6 were nearly simultaneous and there was a roll-up of C_2H_6 due to the competitive adsorption between C_2H_4 and C_2H_6. Zeolite 5A showed the highest adsorption capacity for C_2H_4. When blowdown desorption was conducted in the bed after the adsorption experiment, high C_2H_4 purity could not be obtained because of the strong adsorption of C_2H_4. After blowdown desorption, the purity of C_2H_4 reached close to 90 mol% during vacuum desorption in the zeolite 5A bed.

The breakthrough patterns of the six-component mixture in the zeolite 5A bed were similar to those in the ternary mixture. However, N_2 molecules imparted certain effects on the breakthrough dynamics, which was expected even as it is a relatively weak adsorbate. Moreover, due to the strong adsorption of C_2H_4 and C_3H_6, a large temperature excursion was observed in the adsorption step and a small temperature variation was monitored in the blowdown desorption. In addition, the temperature excursion of the re-adsorption after blowdown desorption showed a small variation of temperature. These results confirmed that zeolite 5A was almost saturated by the strong adsorbates, C_2H_4 and C_3H_6, and blowdown desorption could not remove that which was adsorbed in the pores of Zeolite 5A. Furthermore, a limited vacuum step time and relatively high regeneration pressure are generally applied to the adsorption cyclic processes to save energy and capital cost. As a result, it was not possible to fully regenerate zeolite 5A by the vacuum step in the adsorption cyclic processes.

Based on these results, N_2 and CH_4 molecules may impart a steric hindrance effect on C_2H_4 adsorption at the initial stage of the adsorption step in the zeolite 5A bed. In addition, the adsorption of C_3H_6 can critically affect the overall separation efficiency even though its concentration may be small in the feed. Therefore, a detailed design of the pressure vacuum swing adsorption (PVSA) process is necessary to study the adsorption rate of each component on Zeolite 5A. A product rinse step should also be considered to recover C_2H_4 with high purity from FCC fuel-gas.

ACKNOWLEDGEMENTS

This work was supported by the International Collaborative Energy Technology R&D Program of the Korea Institute of Energy Technology Evaluation and Planning (KETEP) grant funded by the Korean government Ministry of Knowledge Economy (No. 2011T100100425 and No. 2011951010001C).

REFERENCES

1. S. H. Cho, S. S. Han, J. N. Kim, J. H. Park and H. K. Rhee, *Korean*

J. Chem. Eng., **19**, 821 (2002).
2. J. H. Park, S. S. Han, J. N. Kim and S. H. Cho, *Korean J. Chem. Eng.*, **21**, 236 (2004).
3. S. H. Cho, J. H. Park, S. S. Han and J. N. Kim, *Adsorption*, **11**, 145 (2005).
4. R. W. Triebe, F. H. Tezel and K. C. Khulbe, *Gas Sep. Purif.*, **10**, 81 (1996).
5. C. A. Grande, C. Gigola and A. E. Rodrigues, *Ind. Eng. Chem. Res.*, **41**, 85 (2002).
6. M. A. Granato, T. J. H. Vlugt and A. E. Rodrigues, *Ind. Eng. Chem. Res.*, **46**, 7239 (2007).
7. M. Jin, S. S. Kim, Y. D. Kim, J. N. Park, J. H. Kim, C. H. Ko, J. N. Kim and J. M. Kim, *J. Mater. Chem. A*, **1**, 6653 (2013).
8. C. H. Ko, S. S. Han, J. H. Park, S. H. Cho and J. N. Kim, *Ind. Eng. Chem. Res.*, **45**, 9129 (2006).
9. H. W Lee, J. H. Park, S. S. Han, J. N. Kim, S. H. Cho and Y. T. Lee, *Sep. Sci. Technol.*, **39**, 1365 (2004).
10. Y. W. You, D. G. Lee, K. Y. Yoon, D. K. Moon, S. M. Kim and C.-H. Lee, *Int. J. Hydrogen Energy*, **37**, 18175 (2012).
11. S. Ahn, Y. W. You, D. G. Lee, K. H. Kim, M. Oh and C.-H. Lee, *Chem. Eng. Sci.*, **68**, 413 (2012).
12. S. S. Han, J. H. Park, J. N. Kim and S. H. Cho, *Adsorption*, **11**, 621 (2005).
13. Y. H. Kim, D. G. Lee, D. K. Moon, S. H. Byeon, H. W. Ahn and C.-H. Lee, *Korean J. Chem. Eng.*, **31**, 132 (2014).
14. J. G. Jee, S. J. Lee and C.-H. Lee, *AIChE J.*, **51**, 2988 (2005).
15. S. J. Lee, J. J. Hwan, J. H. Moon, J. G. Jee and C.-H. Lee, *Ind. Eng. Chem. Res.*, **46**, 3720 (2007).
16. D. G. Lee, J. H. Kim and C.-H. Lee, *Sep. Purif. Technol.*, **77**, 312 (2011).
17. D. G. Lee, Y. J. Han and C.-H. Lee, *Korean J. Chem. Eng.*, **29**, 1246 (2012).
18. Y. H. Park, D. K. Moon, Y. H. Kim, H. Ahn and C.-H. Lee, *Adsorption*, **20**, 631 (2014).
19. J. W. Carter and H. Husain, *Chem. Eng. Sci.*, **29**, 267 (1974).
20. G. Li, P. Xiao, D. Xu and P. A. Webley, *Chem. Eng. Sci.*, **66**, 1825 (2011).
21. Y.-S. Bae and C.-H. Lee, *Carbon*, **43**, 95 (2005).
22. J. G. Jee, M. B. Kim and C.-H. Lee, *Chem. Eng. Sci.*, **60**, 869 (2005).
23. M.-B. Kim, Y.-S. Bae, D.-K. Choi and C.-H. Lee, *Ind. Eng. Chem. Res.*, **45**, 5050 (2006).
24. X.-Z. Chu, Z.-P. Cheng, X.-X. Xiang, J.-M. Xu, Y.-J. Zhao, W.-G. Zhang, J.-S. Lv, Y.-P. Zhou, L. Zhou, D. K. Moon and C.-H. Lee, *Int. J. Hydrogen Energy*, **39**, 4437 (2014).
25. J. Y. Yang and C.-H. Lee, *AIChE J.*, **44**, 1325 (1998).
26. J. G. Jee, M. B. Kim and C.-H. Lee, *Ind. Eng. Chem. Res.*, **40**, 868 (2001).